PAPER

Red to orange thermally activated delayed fluorescence polymers based on 2-(4-(diphenylamino)-phenyl)-9H-thioxanthen-9-one-10,10-dioxide for efficient solution-processed OLEDs†

Praetip Khammultri, [ID][a] Pongsakorn Chasing,[a] Chirawat Chitpakdee,[b] Supawadee Namuangruk, [ID][b] Taweesak Sudyoadsuk[a] and Vinich Promarak [ID] *[ac]

Most highly efficient thermally activated delayed fluorescence (TADF)-based organic light-emitting diodes (OLEDs) are multi-layer devices fabricated by thermal vacuum evaporation techniques, which are unfavorable for real applications. However, there are only a few reported examples of efficient solution-processed TADF OLEDs, in particular TADF polymer OLEDs. Herein, a series of solution-processable TADF conjugated polymers (**PCTXO/PCTXO-F**x (x = 25, 50 and 75)) were designed and synthesized by copolymerization of 2-(4-(diphenylamino)-phenyl)-9H-thioxanthen-9-one-10,10-dioxide (TXO-TPA) as a red/orange emissive TADF unit, 9,9′-((fluorene-9,9-diyl)-bis(octane-8,1-diyl))-bis(3,6-di-*tert*-butylcarbazole) as host/hole-transporting unit and 2,7-N-(heptadecan-9-yl)carbazole as a conjugated linker and solubilizing group. They possessed a conjugated backbone with donor TPA-carbazole/fluorene moieties and a pendent acceptor 9H-thioxanthen-9-one-10,10-dioxide (TXO) forming a twisted donor–acceptor structure. These polymers in neat films displayed red/orange color emissions (601–655 nm) with TADF properties, proved by theory calculations and transient PL decay measurements. Their hole-transporting capability was improved when the content of 9,9′-((fluorene-9,9-diyl)-bis(octane-8,1-diyl))-bis(3,6-di-*tert*-butylcarbazole) within the polymers increased. All polymers were successfully employed as emitters in solution-processed OLEDs. In particular, the doped OLED fabricated with **PCTXO** exhibited an intense deep orange emission at 603 nm with the best electroluminescence performance (a maximum external quantum efficiency 10.44%, a maximum current efficiency of 14.97 cd A^{-1} and a turn-on voltage of 4.2 V).

Introduction

Thermally activated delayed fluorescence (TADF), recognized as the third-generation light-emitting mechanism for organic light-emitting diodes (OLEDs), has gained a lot of attention over the past few years.[1] Because TADF emissive molecules can reach the theoretical 100% internal quantum efficiency (IQE) by utilizing up-conversion of non-radiative triplet excitons to radiative singlet excitons *via* a reverse intersystem crossing

[a]*Department of Material Science and Engineering, School of Molecular Science & Engineering, Vidyasirimedhi Institute of Science and Technology, Wangchan, Rayong 21210, Thailand. E-mail: vinich.p@vistec.ac.th*

[b]*National Nanotechnology Center (NANOTEC), National Science and Technology Development Agency, Pathum Thani, 12120, Thailand*

[c]*Research Network of NANOTEC-VISTEC on Nanotechnology for Energy, Vidyasirimedhi Institute of Science and Technology, Wangchan, Rayong, 21210, Thailand*

† Electronic supplementary information (ESI) available. See DOI: 10.1039/d1ra04599g

(RISC) process. Considering that they are pure organic molecules, the TADF emitters are capable of effectively tempering the electroluminescent (EL) performance of the phosphorescent OLEDs without the utilization of noble metals. Owing to the synthetic versatility of the organic compounds, moreover, the photophysical and electronic properties of TADF molecules can be fine-tuned by delicately modifying their molecular structures. So far, many TADF materials have been developed using various strategies, such as intramolecular donor–acceptor (D–A) TADF,[2] through-space D–A TADF,[3] excited-state intramolecular proton transfer (ESIPT) induced D–A TADF,[4] organometallic complex TADF,[5] and TADF exciplex.[6] To date, the OLEDs based on TADF emitters can produce the emissive colors covering the whole visible spectrum,[2b,7] especially in the high-energy spectral region (deep-blue emission).[8] For blue and green TADF emitters, the EQE of OLEDs has now exceeded 30%,[9] while that for red TADF emitters has surpassed 25%.[10] Despite the tremendous progress in EL properties of the TADF OLEDs, new TADF materials are still essential to be developed for commercial

applications, in particular, the solution-processable TADF materials, since most of the highly efficient devices are based on small-molecule TADF materials. The inherent physicochemical properties of low solubility, easy crystallization, and poor film-forming ability and morphology of a small-molecule material render most of the efficient small-molecule TADF emitters to be only fabricated by thermal vacuum deposition. Since this thin film deposition technique involves heating a solid material inside a high vacuum chamber at high temperatures and in a small area, it is not suitable for fabricating flexible and large area-size devices. In responding to such requirements, polymers might be a promising alternative. Unlike small molecules, polymeric materials commonly made up of a mixture of different sized molecules can be cast into a high-quality thin film by a solution-based process, such as spin-coating, slot-die coating, and roll-to-roll printing, which is simple, cost-effective, and easy to operate and scale-up for commercial applications. Besides, polymeric emitters have become one of the key findings or developments contributing to the advancement of modern OLEDs since the first report of poly(*p*-phenylene-vinylene) (PPV)-based OLEDs by Friend *et al.* in 1990.[11] Once the TADF concept is introduced into a polymer platform, several types of solution-processable TADF polymers and macromolecules have been designed and synthesized using a variety of tactics, such as conjugated main-chain TADF polymers,[12] non-conjugated main-chain TADF polymers,[13] conjugated side-chain TADF polymers,[1f] non-conjugated side-chain TADF polymers,[14] through-space charge transfer (TSCT) TADF polymers,[15] and dendrimers.[16] However, up till now, only limited examples of TADF polymers have been reported, while their EL efficiencies are still inferior to small-molecule TADF.[2a,17] This could be due to the fact that TADF polymers are more susceptible to suffer triplet–triplet annihilation (TTA) *via* intra- and inter-chain interactions than a small molecule,[18] while it is challenging to concurrently realize a minimal spatial overlap of the highest occupied molecular orbital (HOMO) and lowest unoccupied molecular orbital (LUMO), and a sufficiently small energy gap (ΔE_{ST}) between the lowest singlet (S_1) and triplet (T_1) excited states particularly in the conjugated polymers. These are a couple of recently reported high-performance TADF polymers. Ren *et al.* synthesized a series of conjugated side-chain TADF polymer (Copo1), in which a small-molecule TADF of 2-(10*H*-phenothiazin-10-yl)dibenzothiophene-*S*,*S*-dioxide as a pendant group was attached to the insulating styrene backbone.[14a] Green emitting OLED device based on one of these polymers exhibits a high EQE of over to 20%. Most recently, Wang *et al.* reported the conjugated TADF polymers comprising of small molecular TADF of (4-(9,9-dioctylacridin-10(9*H*)-yl))(4-(9*H*-carbazol-9-yl))benzophenone (AcBPCz) and methyl-substituted phenylene linker.[12e] It was found that the conjugated linkage decreased the local excited triplet state caused by the delocalized polymer backbone. This polymer shows the highest EQE of over 23% with green emission. Despite these progressive improvements in device EL efficiencies, it is still essential and inspiring to realize suitable TADF polymeric emitters for high-performing solution-processed OLEDs.
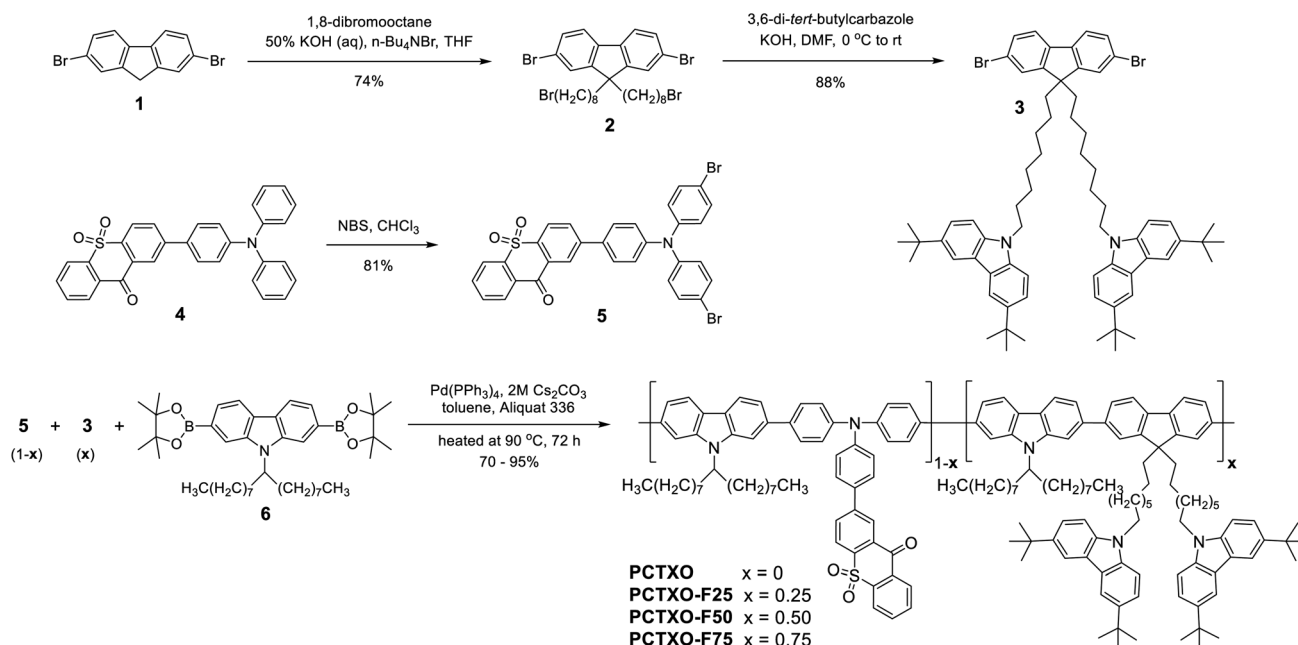
In this study, therefore, a series of conjugated main-chain polymers were designed and synthesized based on a classical small-molecule TADF of 2-(4-(diphenylamino)-phenyl)-9*H*-thioxanthen-9-one-10,10-dioxide (TXO-TPA).[19] In these polymers, the TXO-TPA unit was implanted into the backbone by copolymerization with 2,7-*N*-(heptadecan-9-yl)carbazole and 9,9′-((fluorene-9,9-diyl)-bis(octane-8,1-diyl))-bis(3,6-di-*tert*-butyl-carbazole) through the diphenylamino group of its triphenyl-amine (TPA) donor moiety, forming a backbone-donor/pendant-acceptor type π-conjugated TADF polymer (Scheme 1). In this design, both carbazole and fluorene as comonomers will provide a rigid π-conjugated polymer backbone which could suppress a non-radiative decay giving rise to the enhancement of the photoluminescence efficiency while linking *via* their 2,7 positions will not strongly affect the donor property of the TXO-TPA unit. Furthermore, the 2,7-*N*-(heptadecan-9-yl)carbazole comonomer is also intended to act as a linker capable of the hole-transporting channel and improving the solubility of the polymers. It has been reported that branched *N*-alkyl-substituted-carbazole-2,7-diyl-based copolymers with high molecular weight demonstrate high hole-transporting ability and good processability.[20] Besides, the grafted 3,6-di-*tert*-butyl-carbazole units on the side chain of the comonomer would also enable the hole-transporting ability and the host without altering the electronic properties of the polymer backbone as it has been noticed in some of its derivatives.[1f,21] By managing the content of the 9,9′-((fluorene-9,9-diyl)-bis(octane-8,1-diyl))-bis(3,6-di-*tert*-butylcarbazole) unit in the polymers, series of TADF polymers with tuning optical and electronic properties, namely **PCTXO** and **PCTXO-F*x*** (*x* represents the molar content of this fluorene monomer) were attained (Scheme 1). Indeed, all polymers exhibit TADF property with an improved hole-transporting capability as the content of *x* increased. The red/orange TADF polymer OLED peaked at 603 nm reaches an EQE_{max} of over 10% and an current efficiency (CE_{max}) of 14.97 cd A^{-1}.

Results and discussion

Synthesis and characterizations

The designed TADF polymers were synthesized *via* Suzuki cross-coupling polycondensation between relevant 2-(4-(bis(4-bro-mophenyl)amino)phenyl)-9*H*-thioxanthen-9-one-10,10-dioxide (**5**), 9,9′-((2,7-dibromofluorene)-bis(octane-8,1-diyl))-bis(3,6-di-*tert*-butylcarbazole) (**3**) and 9-(9-heptadecanyl)-2,7-bis(4,4,5,5-tetramethyl-1,3,2-dioxaborolan-2-yl)carbazole (**6**) monomers, as described in Scheme 1. The monomer **5** was prepared in good yield from an NBS bromination of its precursor **4**. The monomer **3** was synthesized by alkylation of dibromofluorene **1** with an excess of 1,8-dibromooctane in the presence of KOH followed by a nucleophilic substitution reaction of the resultant **2** and 3,6-di-*tert*-butylcarbazole catalyzed by KOH. In the polymerization, three monomers **5**, **3** and **6** were fed in different molar ratios of 1 : 0 : 1, 0.75 : 0.25 : 1, 0.50 : 0.50 : 1, and 0.25 : 0.75 : 1 in the presence of Pd(PPh$_3$)$_4$/Cs$_2$CO$_3$(aq.) as catalysts in toluene/Aliquat at 90 °C. The resulting polymers denoted as **PCTXO** and **PCTXO-F*x*** (*x* = 25, 50 and 75) were subjected to sequential

Scheme 1 The synthesis and structures of polymers **PCTXO** and **PCTXO-Fx** (x = 25, 50, and 75).

Soxhlet extraction with acetone and chloroform and purified to remove unreacted monomer and low molecular weight species as well as the reaction catalyst to afford red to orange solids in 70–95% yields, respectively. The chemical structures of these polymers were verified by proton nuclear magnetic resonance (^{1}H NMR) and Fourier-transform infrared spectroscopy (FTIR) analysis, as depicted in Fig. 1 (Fig. S1, ESI†). In terms of structural characterization, the contents of monomers **5** and **3** in each polymer could be quantified using both ^{1}H NMR and FTIR

spectra. As shown in Fig. 1, by comparing the ^{1}H NMR spectra of **PCTXO-Fx** to that of **PCTXO**, it can be noticed that the signal peaks at chemical shifts of 8.06 (d), 4.11 (a), 2.12 (b) and 1.73 ppm (c) originated from the characteristic protons of monomer **3** are visible, confirming the existence of this monomer in the polymers. Meanwhile, the signal peaks derived from the protons of the monomers **5** and **6** are observed at chemical shifts of 8.57 (g) and 8.38 ppm (i), and 4.69 (e) and 0.79 ppm (f) in all cases, respectively. The intensities of protons (g) and (i) of
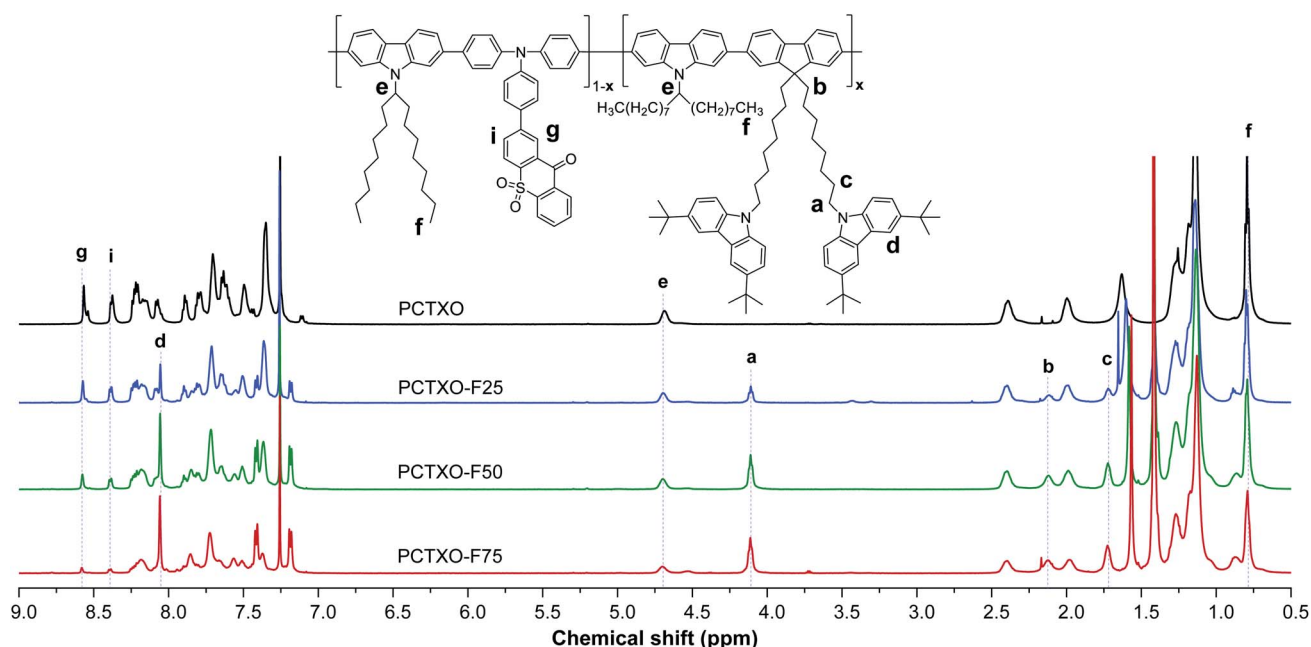

Fig. 1 600 MHz ^{1}H-NMR spectra (CDCl$_3$) of polymers **PCTXO** and **PCTXO-Fx** (x = 25, 50 and 75).

monomer **5** decrease gradually with the decrease in the percentage of monomer **5** in the polymers. The actual molar ratios of monomer **3** in the polymers were estimated from analysis of their ^{1}H NMR spectra (Fig. S2, ESI†) to be 23.5%, 50.3%, 76.1% for **PCTXO-F25**, **PCTXO-F50**, **PCTXO-F75**, respectively, which is in good agreement with the feed amount of monomer **3**. Analysis of the FTIR spectra of these polymers also revealed that the relative intensities of absorption peaks of C=O (1590 cm^{-1}) and O=S=O groups (1303 and 1153 cm^{-1})[22] came from the monomer **5** slowly decreased, while the relative intensities of absorption peaks of alkyl groups (2920 and 2851 cm^{-1}) progressively increased (Fig. S1, ESI†), proving that the synthesized polymers contained various monomer proportions. The number-average molecular weight (M_n) and polydispersity indices (PDI) of **PCTXO** and **PCTXO-Fx** were determined by gel permeation chromatography (GPC) eluting with THF to be 11.71–21.65 kDa and 2.21–2.39, respectively (Table 1 and Fig. S3, ESI†). It is noted that the M_n values of these polymers are increased with the increased percentage of monomer **3** units. Owing to the existence of alkyl chains, **PCTXO** and **PCTXO-Fx** can be dissolved nicely in common polar organic solvents, such as toluene, dichloromethane, chlorobenzene, and THF, which is helpful to form good-quality thin film using solution processing.

Theoretical calculation

In order to evaluate the effect of the comonomer on the TXO-TPA TADF unit in the polymer backbone, the HOMO and LUMO distributions and S_1 and T_1 energies of the four polymer fragments (**A**, **B**, **C**, and **D**) consisting of a TXO-TPA unit and its adjacent carbazole/TPA moieties were calculated by the time-dependent density functional theory (TD)-B3LYP/6-31g(d) and the Tamm–Dancoff approximation (TDA)-M062X/6-31G(d) methods, respectively.[23] As shown in Fig. 2, in all cases, the LUMO orbitals are localized entirely on the electron acceptor 9*H*-thioxanthen-9-one-10,10-dioxide (TXO) moiety, while a clear difference in the distribution of the HOMO orbital is seen in the polymer fragments. For fragment **A**, the HOMO orbitals are distributed on the donor TPA moiety and spread over the adjacent carbazole units and slightly on the adjoining phenyl ring of the TXO unit. However, by further copolymerization of the repeating fragment **A** with monomer **3** forming fragment **B**, the two connected fluorene rings to **A** barely makes any effect in the distribution of the HOMO, while the distribution of the HOMO is spread over the central TPA (TPA-TXO) and the two carbazole-TPA moieties in the fragment **C** when **A** is further polymerized with monomer **5**. For fragment **D**, where **A** is copolymerized with both monomers **3** and **5**, the HOMO orbitals holding a feature of both **B** and **C** are delocalized on the central TPA and the carbazole-TPA moiety with no contribution from the fluorene unit from another side. Hence, the TADF emissive features of the polymers largely depend on the fragment comprising of **A** and its adjacent TPA unit. According to the calculated HOMO and LUMO energy levels of **A–D** (Fig. 2), there are roughly two possible TADF fragments of **A/B** and **C/D** that could be responsible for the TADF property in the

Table 1 Optical, physical and electronic data of polymers PCTXO and PCTXO-Fx (x = 25, 50 and 75) in solution and thin film

Polymer	M_n/PDI[a]	λ_{abs} (nm) sol[b]/nf[c]	λ_{em} (nm) sol[b]/nf[c]	Φ_{PL}[e] (%) sol[b]/nf[c]/df[d]	τ^f (ns) sol[b]/nf[c]/df[d]	τ^i (μs) sol[b,g](sol[b,h])/nf[c]	E_g^{opt}[j] (eV)	HOMO/LUMO[k] (eV)	ΔE_{ST}[l] (eV)	μ_h^m (cm² V⁻¹ s⁻¹)
PCTXO	11 713/2.21	378/384	605/655/590	22/25/78	3.1(17.4)/8.2	12.5 (90.3%)/47.9 (9.7%)	2.32	−5.50/−3.18	0.15	1.35 × 10⁻⁷
PCTXO-F25	15 628/2.39	380/386	603/641/586	19/21/70	4.0(13.4)/16.7	11.0 (87.8%)/42.9 (12.2%)	2.37	−5.53/−3.16	0.13	3.86 × 10⁻⁷
PCTXO-F50	17 324/2.37	381/387	602/622/583	32/27/81	3.3(22.0)/24.1	12.3 (85.7%)/48.1 (14.3%)	2.43	−5.56/−3.13	0.12	8.22 × 10⁻⁶
PCTXO-F75	21 648/2.34	382/389	602/601/572	26/28/71	3.7(30.6)/32.3	11.1 (77.8%)/47.4 (22.2%)	2.45	−5.69/−3.24	0.12	1.36 × 10⁻⁵

^{a} Determined by GPC, eluting with THF, by comparison with polystyrene standards. ^{b} Recorded in toluene solution (10^{-6} M). ^{c} Measured as polymer 5 wt% doped mCP films coated on fused silica substrates. ^{d} Measured as neat film coated on fused silica substrates. ^{e} Absolute photoluminescence quantum yield measured using an integrating sphere in air. ^{f} Prompt fluorescence lifetime measured in ambient conditions. ^{g} Obtained in air-saturated conditions. ^{h} Obtained in degassed conditions. ^{i} Delayed fluorescence lifetime measured as polymer 5 wt% doped mCP films at 300 K. ^{j} Deduced from the absorption onset of a neat film: E_g^{opt} = 1240/λ_{onset}. ^{k} HOMO measured by AC-2 of a neat film and LUMO = HOMO + E_g^{opt}. ^{l} Excited singlet–triplet energy gap (ΔE_{ST}) obtained from the fluorescent and phosphorescent spectra of 1 wt% polymer blended Zeonex films measured at 300 K and 77 K, respectively. ^{m} Hole mobility (ITO/PEDOT:PSS (35 nm)/polymer (130 nm)/MoO₃ (10 nm)/Al (80 nm)).
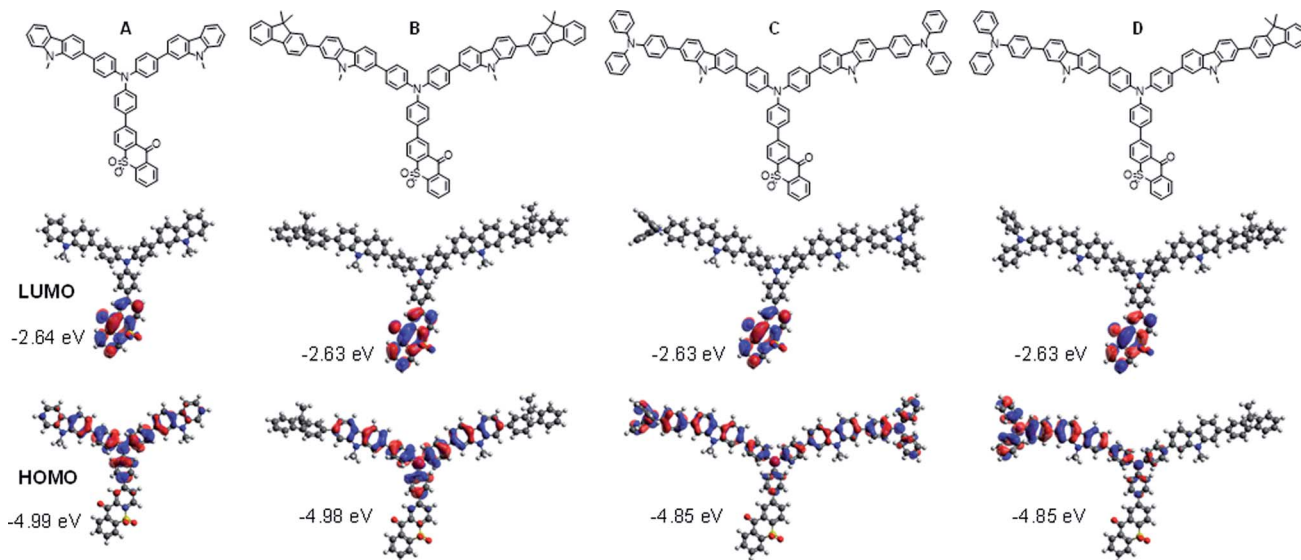
Fig. 2 Molecular structures, and frontier orbital distributions of HOMO and LUMO of the polymer fragments (**A**–**D**) calculated by DFT-B3LYP/6-31g(d) method.

polymers. Besides, there is a slight overlap between both orbitals of the fragments, suggesting that the HOMO → LUMO transition possesses a strong intramolecular charge transfer (ICT) between the donor and acceptor parts, which is beneficial for enhancing the photoluminescence efficiency due to the escalating radiative rate from the overlap.[1c] Such effective HOMO–LUMO separation can also induce a small electron exchange energy. The calculated ΔE_{ST} values of **B** and **C** were 0.15 and 0.26 eV, respectively, which are somewhat higher than that of its original small-molecule, TXO-TPA (ΔE_{ST} = 0.04–0.09 eV).[19,24] This could be ascribed to a noticeable π-electron conjugation between the TXO-TPA and the comonomers in the ground state.

Photophysical properties

The UV-vis absorption and photoluminescence (PL) spectra of **PCTXO** and **PCTXO-F***x* in both toluene and neat film are given in Fig. 3, and their photophysical data are listed in Table 1. In solution, all four polymers showed an intense absorption band peaked at ~378–382 nm, correlating to the π–π* transition of the conjugated polymer backbone,[25] whereas a peak at ~299 nm is only clearly seen in the spectra of **PCTXO-F***x*, which corresponds to π–π* transition of the carbazole unit in the monomer **3** (Fig. 3a). Besides, a much less intense broad absorption band at >420 nm could be assigned to the CT absorption, which is similarly observed in the absorption spectrum of the TXO-TPA TADF molecule.[19,24] The intensity of this band gradually decreased with a decrease in the content of the monomer **5** unit in the polymers. Their PL spectra in toluene displayed single CT emission bands from the TADF emissive unit at ~603 nm when excited at ~400 nm (corresponding to the absorption peak of polymer backbone), indicating an efficient intra- and intermolecular charge transfer from the conjugated backbone to the TADF fragment.[26] A similar phenomenon was also noticed for

the polymers in neat films, as described in Fig. 3b. This also means that the excited energy levels (LUMO or S_1/T_1) of the incorporated copolymer fragment match well with those of the emissive TADF one allowing an energy transfer to take place with very high efficiency. Thus, in the designed polymers, the comonomer of 9,9'-((fluorene-9,9-diyl)-bis(octane-8,1-diyl))-bis(3,6-di-*tert*-butylcarbazole) (monomer **3**) can act as successful support for the organization of the host matrix for the TADF unit along with the conjugated copolymer backbone. In film

Fig. 3 UV-Vis absorption and PL spectra of the polymers in (a) toluene and (b) as neat film.

state, both UV-vis absorption and PL spectra of polymers were red-shifted towards the longer wavelength compared to their corresponding spectra in solution (Table 1). Besides, the emission peaks were steadily blue-shifted with a decrease in the TADF unit (monomer **5**) content, owing to aggregation in the condensed solid state. These photophysical phenomena are also identical to previous reports on the conjugated copolymers comprising a long-wavelength emissive unit.[12a,c,27]

In toluene solution under ambient conditions, all polymers were moderate emitters with absolute photoluminescence quantum yield (Φ_{PL}) of 19–32% (Table 1). The transient PL decay plots indicated a short mean PL lifetime ($\tau = 3.1$–4.0 ns) without noticeably delayed fluorescence. However, both PL emission intensities and PL lifetimes of the polymer solutions under degassed conditions were significantly higher and longer ($\tau = 13.4$–30.6 ns) than in air-saturated environments, respectively (Fig. 4a, b, S4, ESI† and Table 1). This is because of the suppression of the oxygen quenching effect on the triplet state, signifying the delayed fluorescence character. As shown in Fig. 4c, the transient PL decay spectra of the polymer in the neat film display a longer PL lifetime relative to those in the solution (Table 1). Notably, these τ values incredibly increased with the increasing content of monomer **3** in the polymers from $\tau = 8.2$ ns for **PCTXO**, $\tau = 16.7$ ns for **PCTXO-F25**, $\tau = 24.1$ ns for **PCTXO-F50** to $\tau = 32.2$ ns for **PCTXO-F75**. This suggests that the presence of 9,9′-((fluorene-9,9-diyl)-bis(octane-8,1-diyl))-bis(3,6-di-*tert*-butylcarbazole) (monomer **3**) as copolymer has the capability of suppressing aggregation quenching between the TADF emissive fragments presumably due to its crowded

molecular structure and molecular rigidity in the conjugated backbone. To further study the TADF characteristics of **PCTXO** and **PCTXO-F***x*, the transient PL decay measurements were performed on 5 wt% doped mCP films at room temperature (Fig. 4d and S5, ESI†). All spectra displayed double exponential decay of the nanosecond-scale prompt fluorescence (PF) and the microsecond-scale delayed fluorescence (DF). As a result, their Φ_{PL} values (70–81%) in doped mCP films were considerably higher than those in solution and neat film (Table 1). The microsecond-scale or TADF decay is a multi-exponential that can be roughly split into two components (Fig. 4d and S5, ESI†). The fast component (77.8–90.3%) of TADF has a single-exponential decay time in the range of 11.0–12.5 μs, while the slow one (9.7–22.2%) has a single-exponential decay time in the range of 42.9–48.1 μs (Table 1). The two TADF components appear to arise from two different TADF fragments in the doped film because of the different spectra observed for these two components (Fig. 4d inset). This result is well consistent with a previous observation in the theoretical calculations. Two sets of TADF fragments (**A/B** and **C/D**) can contribute to the TADF emissions in the polymers. Notably, these DF lifetime values (42.9–48.1 μs) are somewhat lower than that of the TXO-TPA TADF small molecule (78.0 μs),[19] probably due to the extended conjugation in the HOMO of the TADF part.[28] Furthermore, the polymers were also characterized by the temperature-dependent transient PL decay measurements of the polymers doped mCP:Zeonex films from 100 to 300 K (Fig. 4e and S6, ESI†). All of them obviously display the PF and DF components. The DF intensity increases with the increase in temperature from 100 to
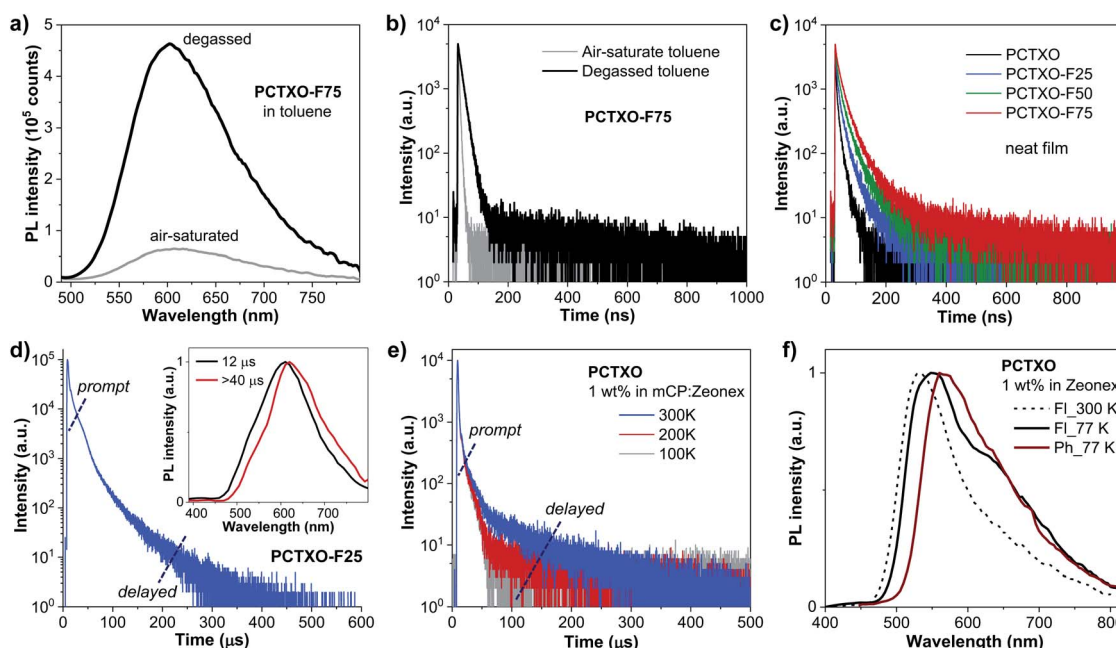

Fig. 4 (a) PL spectra and (b) transient PL decay spectra of air-saturated and degassed **PCTXO-F75** toluene solutions. (c) Transient PL decay spectra of the polymer as neat films. (d) Transient PL decay spectra of **PCTXO-F25** 5 wt% doped mCP films at room temperature (inset: PL spectra of TADF components at 12 μs and >40 μs). (e) Transient PL decay spectra of **PCTXO** 1 wt% doped in mCP:Zeonex film recorded at various temperatures in N$_2$. (f) Fluorescence (Fl) and phosphorescence (Ph) spectra of **PCTXO** 1 wt% doped in Zeonex film recorded at 300 K and 77 K. The wide impulse response function (micro flash lamp) causes the distortion of the prompt component in the decay spectra of (d) and (e).

300 K, suggesting that the up-conversion from T_1 to S_1 states is activated by supplying thermal energy. This phenomenon corroborates that **PCTXO** and **PCTXO-Fx** are TADF emitters.

To ensure the TADF properties of **PCTXO** and **PCTXO-Fx**, the phosphorescent (Ph) and fluorescent (Fl) spectra of the 1 wt% doped in Zeonex films were recorded at 77 K, as shown in Fig. 4f and S7 (ESI†). By taking the maximum peak wavelengths of the Ph spectra to determine the triplet energy (E_T) and the maximum peak wavelengths of the Fl spectra to calculate the singlet energy (E_S), the ΔE_{ST} values were estimated to be in the range of 0.12–0.15 eV, which are beneficial for efficient TADF (Table 1). Such a relatively small ΔE_{ST} value (<0.2 eV) is one of the crucial obligations to accomplish an efficient reverse intersystem crossing (RISC) process from the T_1 to S_1.

Thermal, electrochemical, charge transport and morphological properties

The thermal properties of **PCTXO** and **PCTXO-Fx** were investigated by TGA and DSC under a nitrogen atmosphere at a heating rate of 10 °C min^{-1}. All polymers showed good thermal stability with high decomposition temperatures (T_d, with 5% weight loss) of 358–432 °C and glass transition temperatures (T_g) of 112–158 °C (Fig. S8, ESI†). Moreover, no apparent exothermic crystallization and endothermic melting peaks over the heating range were detected in the DSC traces, suggesting that the crystallization of TADF units is suppressed by the comonomer units in the polymer backbone.

The electrochemical behavior of these polymers was studied by cyclic voltammetry (CV) in an argon-saturated anhydrous dichloromethane solution containing 0.1 M n-Bu$_4$NPF$_6$ as a supporting electrolyte. As depicted in Fig. 5a, all polymers exhibit two quasi-reversible and one reversible reduction process. The reduction wave of all four polymers occurred at the same reduction half-wave potential ($E_{1/2}$) of ~ -1.04 V, which

could be attributed to a radical anion formation of the carbonyl oxygen atoms of the TXO moiety.[29] The first oxidation wave at $E_{1/2}$ of ~ 0.91 V could be ascribed to the generation of radical cations on a donor moiety of the TADF fragment, while the second oxidation wave at $E_{1/2}$ of ~ 1.11 V observed in the polymers **PCTXO-Fx** could be assigned to the oxidation of the 3,6-di-*tert*-butylcarbazole pendant in the comonomer 3.[21] Apparently, as the content of monomer 5 in the polymers is reduced from **PCTXO** to **PCTXO-F75**, the currents of both reduction and first oxidation waves are steadily decreased, whereas the current of the oxidation wave at 1.11 V is gradually enhanced. The HOMO energy levels of **PCTXO** and **PCTXO-Fx** in film state were then measured by UV photoelectron spectroscopy in air (Model AC-2) to be −5.50, −5.53, −5.56, and −5.69 eV, respectively (Table 1 and Fig. S9, ESI†). From the HOMO values and the optical band gap energies (E_g^{opt}) estimated from an absorption onset value of the neat film UV-vis absorption spectra, the LUMO levels of these polymers were deduced to be in the range of −3.13 to −3.24 eV (Table 1).

To evaluate the hole-transporting property of these polymers, the hole-only device (HOD) was fabricated with the structure of ITO/PEDOT:PSS (35 nm)/polymer (130 nm)/MoO$_3$ (10 nm)/Al (80 nm), where MoO$_3$ was employed to ensure that only hole carrier is injected and transported in the device due to its work function of 6.90 eV being high enough to block electron injection from the Al cathode.[30] The hole motility (μ_h) of each polymer was estimated by means of the space-charge-limited current (SCLC) method and extracted by fitting the J–V curves in the SCLC regime where the applied voltage range follows the Mott–Gurney model (Fig. 5b).[31] The μ_h values were calculated to be in the range of 1.35×10^{-7} to 1.36×10^{-5} cm^2 V^{-1} s^{-1} (Table 1). The hole-transporting ability of the polymers is improved as the content of comonomer 3 in their conjugated backbone increased. It is well understood that superior hole mobility can be profitable for a high-performance OLED device since higher charge mobility through the emitter could provide a wider recombination zone in an emissive layer (EML) and lead to a longer device lifetime as well as lower driving voltages.[32]

Electroluminescence properties

To explore the potential application of these TADF polymers as the emitters for solution-processed OLEDs, the non-doped devices (I–IV) were firstly fabricated with the optimized architecture of ITO/PEDOT:PSS (35 nm)/polymers (60 nm)/TmPyPB (40 nm)/LiF (0.5 nm)/Al (100 nm), where poly(3,4-ethylenedioxythiophene):poly(styrene sulfonate) (PEDOT:PSS) and 1,3,5-tri(m-pyrid-3-yl-phenyl) benzene (TmPyPB) serves as the hole injection layer and the hole- and electron-transporting layer, respectively. The neat films of **PCTXO** and **PCTXO-Fx** as the emissive layer (EML) are spin-coated from chlorobenzene solution. As shown in Fig. 6a, the OLEDs (device I–IV) exhibit their inherent emissions with similar emissive wavelengths to PL spectra of the neat films. The device (I) using **PCTXO** as EML gave saturated red electroluminescence centered at 662 nm with the satisfied color coordinates of CIE (0.63, 0.36). Markedly, the emissive wavelengths of this **PCTXO**-based OLED showed a red-
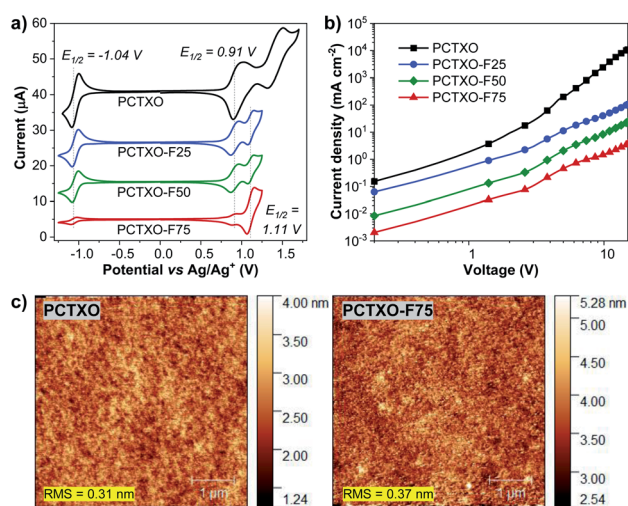

Fig. 5 (a) Cyclic voltammograms of the polymers in dichloromethane solutions measured at a scan rate of 50 mV s^{-1}. (b) Current density–voltage (J–V) plots of the hole only device (ITO/PEDOT:PSS (35 nm)/polymer (130 nm)/MoO$_3$ (10 nm)/Al (80 nm)). (c) AFM images of PCTXO and PCTXO-F75 5 wt% doped in mCP films.
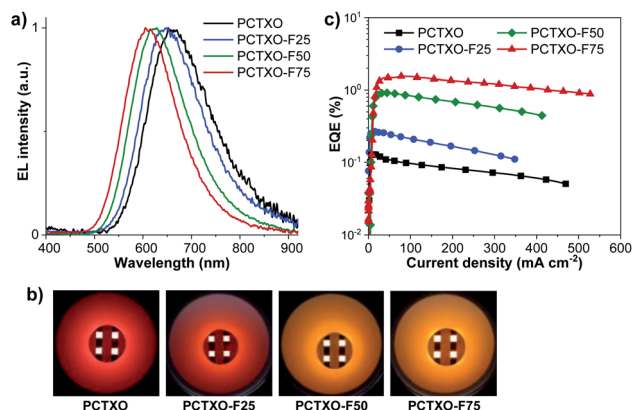
Fig. 6   (a) Normalized EL spectra, (b) EQE–current density plots, and (c) photographs of the non-doped OLEDs (devices I–IV) based on **PCTXO** and **PCTXO-F**x.

shifted EL with respect to those of the TXO-TPA[19] and its TADF polymeric emitters.[12a,c] The emission colors of the devices gradually blue-shifted as the ratio of monomer **5** in the polymers decreased, as illustrated in Fig. 6b. The **PCTXO-F75**-based OLED (device IV) emitted orange emission peaked at 611 nm with CIE coordinates (0.55, 0.44). Clearly, among these four polymers, the **PCTXO-F75** (device IV) achieved the best device EL performance showing both the highest maximum external quantum efficiency (EQE_{max}) of 1.54% and the lowest turn-on voltage (V_{on}) of 5.1 V. The EL performance of these non-doped OLEDs (device I–IV) (CE, and EQE_{max} values) increases in the order of I < II < III < IV (Fig. 6c and Table 2), correlated well with the hole mobility of their corresponding emissive polymers, which is observed to be **PCTXO-F75** > **PCTXO-F50** > **PCTXO-F25** > **PCTXO** (Table 1). Unfortunately, the EL efficiencies of these non-doped devices were still inferior, with EQE_{max} values in the range of 0.13–1.54%, considering that they were fabricated with TADF emitters. This is presumably due to the imbalanced charge injection and transport and aggregation-caused quenching (ACQ) owing to high proportions of TADF units in the neat films, consistent with their low thin-film Φ_{PL} values.

To attain the optimal TADF properties of the synthesized polymers in the device, OLEDs were fabricated using the

polymer doped mCP films as the EML (Fig. 7a). The device structure was ITO/PEDOT:PSS (35 nm)/EML (60 nm)/TmPyPB (40 nm)/LiF (0.5 nm)/Al (100 nm), where the EML was spin-coated from **PCTXO**/**PCTXO-F**x:mCP in chlorobenzene solution. The doping concentration ratio between the polymers and mCP host material was initially optimized by varying from 1 wt% to 20 wt%. Fig. S11 (ESI†) presents PL and transient PL decay spectra of all polymers doped in mCP. The films containing polymer 5 wt% doped in mCP exhibited the highest Φ_{PL} values of 70–81% (Table 1) with the PL spectra purely represent the emission of the polymer, indicating an effective energy transfer from the host to dopant. In comparison to their PL in the neat film, these PL spectra are somewhat blue shifts (29–65 nm), suggesting that diluting of the polymers in mCP host well repress intra-/inter-polymer chain aggregation and interactions in the film state. Furthermore, in all cases, the transient PL decay spectra obviously displayed both PF and DF components, signifying the existence of the TADF feature in the doped film. To assess the morphological stability and the compatibility of the polymers in the mCP matrix, the surface of these doped films was examined by atomic force microscopy (AFM). As shown in Fig. 5c (Fig. S12, ESI†), all thin films display smooth and homogeneous film morphologies with no pinholes and crystalline islands. The root-mean-square (RMS) roughness values were in the range of 0.31–0.42 nm, indicating high-quality nanoscale thin films.

The EL characteristics and parameters of the doped devices (V–VIII) are shown in Fig. 7 and are summarized in Table 2, respectively. Remarkably, all fabricated OLEDs (device V–VIII) exhibited a significant enhancement in the EL performances compared with those of their corresponding non-doped devices (I–IV). Such superior EL performances in the doped devices imply that the TADF facet of the polymers and their triplet excitons could be effectively utilized in the dispersed dopant/host systems. As illustrated in Table 2, the EL properties (EQE_{max}, CE_{max}, and V_{on}) of the devices (V–VIII) tend to drop steadily as the ratio of monomer **5** in the polymer decreases, probably due to a reduction in the proportions of TADF fragments in the EML. Nevertheless, the EQE_{max} values of these devices were over a theoretical limit of 5% for the efficiency of the conventional fluorescent OLEDs, certainly demonstrating

Table 2   Electroluminescent data of OLEDs fabricated with TADF polymers **PCTXO** and **PCTXO-F**x (x = 25, 50 and 75)

Device	Polymer	V_{on} (V)	λ_{EL} (nm)	L_{max} (cd m^{-2})	J_{max} (mA cm^{-2})	FWHM (nm)	CE_{max}^{c} (cd A^{-1})	EQE_{max} (%)	CIE (x, y)
I[a]	**PCTXO**	8.6	662	319	348	158	0.19	0.13	0.63, 0.36
II[a]	**PCTXO-F25**	6.2	648	302	447	148	0.20	0.27	0.62, 0.38
III[a]	**PCTXO-F50**	5.7	624	1617	389	136	0.51	0.92	0.58, 0.41
IV[a]	**PCTXO-F75**	5.1	611	1447	501	130	0.88	1.54	0.55, 0.44
V[b]	**PCTXO**	4.2	603	6836	273	117	14.97	10.44	0.56, 0.43
VI[b]	**PCTXO-F25**	5.6	600	6987	274	121	11.98	7.86	0.54, 0.45
VII[b]	**PCTXO-F50**	5.8	596	4696	249	121	10.06	6.31	0.52, 0.46
VIII[b]	**PCTXO-F75**	6.2	587	7008	209	121	9.72	5.10	0.50, 0.48

[a] ITO/PEDOT:PSS (35 nm)/polymer (60 nm)/TmPyPB (40 nm)/LiF (0.5 nm)/Al (100 nm). [b] ITO/PEDOT:PSS (35 nm)/polymer 5 wt% doped mCP (60 nm)/TmPyPB (40 nm)/LiF (0.5 nm)/Al (100 nm). [c] Maximum current efficiency.
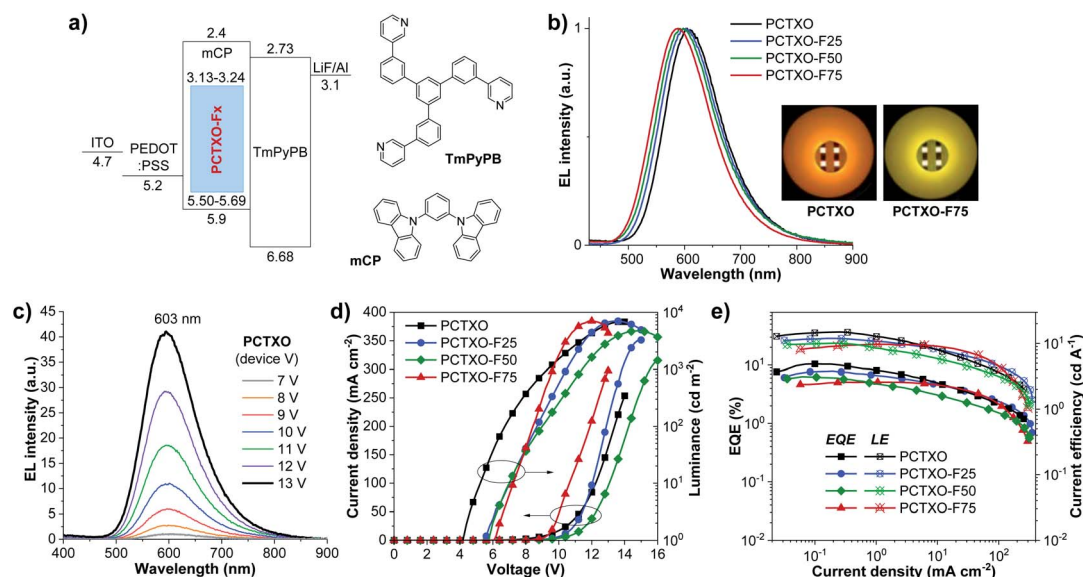
Fig. 7 (a) Energy level diagram of the OLEDs and organic materials used in this study. (b) Normalized EL spectra (Inset: photographs of **PCTXO** and **PCTXO-F75**-based OLEDs (devices V–VIII)). (c) EL spectra of **PCTXO**-based OLED (device V) at different applied voltages. (d) Current density–voltage–luminance (J–V–L) characteristics and (e) EQE–current density–current efficiency plots of the doped OLEDs (devices V–VIII) based on **PCTXO** and **PCTXO-F**x.

the efficient RISC contribution from the TADF fragments in the polymers. Among them, the device V using **PCTXO** 5 wt% doped mCP as an EML showed the best EL performance with an EQE_{max} of 10.44%, a maximum current efficiency (CE_{max}) of 14.97 cd A^{-1}, a V_{on} of 4.2 V, and a luminescence over 6836 cd m^{-2}. This OLED gave a deep orange EL emission with the peak wavelength at 603 nm and color coordinates of CIE (0.56, 0.43) (Fig. 7b). The **PCTXO-F25**-based device (VI) exhibited a bit lower EL property with EQE_{max}/CE_{max} values of 7.86%/11.98 cd A^{-1}, a V_{on} of 5.6 V, and a luminescence over 6987 cd m^{-2} at the peak wavelength of 600 nm. Device VIII based on 5 wt% **PCTXO-F75** doped mCP having the minor content of the TADF unit in the film delivered the lowest EL performance with EQE_{max}/CE_{max} values of 5.10%/9.72 cd A^{-1} and deep yellow EL emission peaking at 587 nm. In addition, the EL spectra of all doped devices (V–VIII) showed single peak emissions, which coincided nicely with the PL profiles of the EML. This result clearly demonstrates the complete transfer of energy from the mCP host/polymer conjugated backbone to the TADF emissive units. Their EL spectra were not also influenced by the changes in the applied voltages over the 7–13 V range, as shown in Fig. 7c (Fig. S13, ESI†), meaning that these fabricated devices are not suffered by the excimer or exciplex emissions from EML/TmPyPB interface and possess excellent operating stability. To the best of our knowledge, the EL performance of **PCTXO**-based device (V) is one of the best achieved based on TXO-TPA derivatives by solution-process technique so far.[12a,c,24] Although its EQE of 10.44% is moderate compared with the reported state-of-the-art multi-layer thermally evaporated small-molecule TADF-based OLEDs,[1a,10b,19,33] this OLED offers a straightforward device structure (only two organic layers) with a low-cost fabrication process, which is suitable for a practical application.

Conclusions

In summary, a series of red/orange emissive TADF conjugated polymers **PCTXO/PCTXO-F**x (x = 25, 50 and 75) have been designed and synthesized by Suzuki coupling polycondensation, in which 2-[4-(diphenylamino)phenyl]-9H-thioxanthen-9-one-10,10-dioxide (TXO-TPA) as a red/orange emissive TADF unit was polymerized with 2,7-carbazole as host and solubilizing component via its TPA donor moiety forming a backbone-donor/pendant-acceptor type TADF polymer. The TADF behaviours were tuned by copolymerization of TXO-TPA with 9,9′-((fluorene-9,9-diyl)-bis(octane-8,1-diyl))-bis(3,6-di-tert-butylcarbazole) as host/hole-transporting unit in various ratios. Photophysical and theoretical data verified that all polymers possess efficient TADF characteristics with small ΔE_{ST} values (0.12–0.15 eV). All polymers exhibited a single emission band from the TADF component with emission colors ranging from saturated red to orange. Their hole-transporting abilities steadily improved as the content of the 9,9′-((fluorene-9,9-diyl)-bis(octane-8,1-diyl))-bis(3,6-di-tert-butylcarbazole) in the backbone increased. As a result, the solution-processed OLED fabricated with **PCTXO-F75** as a non-doped emissive layer showed the best device electroluminescence (EL) property with a maximum external quantum efficiency (EQE_{max}) of 1.54%. Further doping these polymers (5 wt%) in mCP host was significantly enhanced the EL performances of their OLED devices. All solution-processed OLEDs showed high EQE_{max} values of over 5%. Particularly, the doped device employing **PCTXO** as the emitter attained the finest EL results (an EQE_{max} of 10.44%, a maximum current efficiency of 14.97 cd A^{-1}, a V_{on} of 4.2 V) with an intense orange color emission peaked at 603 nm. These findings demonstrate a helpful design strategy to

enhance the TADF performance of TXO-TPA-based red/orange emissive materials for highly efficient solution-processed OLEDs and will be a valuable guide for the further development of new polymeric TADF materials.

Experimental

Materials and methods

All chemicals were purchased from Tokyo Chemical Industry and Sigma-Aldrich and used without further purification. Solvents were dried using standard techniques.

The polymers were confirmed molecular weight by gel permeation chromatography (GPC) on Malvern's Viscotek TDAmax using THF as a solvent system and polystyrene (PS) as a standard material. ^{1}H-NMR and ^{13}C-NMR spectra were recorded on Bruker AVANCE III HD 600 MHz. IR spectra were carried out on PerkinElmer model Frontier FT-IR, Universal-ATR. High-resolution mass spectrometry (HRMS) was performed on Bruker Autoflex speed MALDI-TOF mass spectrometer (MALDI-TOF-MS). Thermogravimetric analysis (TGA) was performed on Rigaku model Thermoplus TG8120 under N_2 flow at a heating rate of 10 °C min^{-1}. Differential scanning calorimetry (DSC) was recorded on PerkinElmer model Lab System-DSC-8500 under N_2 flow at a heating rate of 10 °C min^{-1}. UV-vis absorption spectra of solution and neat film were performed on PerkinElmer model Lambda 1050. Fluorescence and phosphorescence spectra were recorded on the Edinburgh fluorescence spectrometer (FLS980). The absolute photoluminescence quantum yields (Φ_{PL}) of solution and film were measured by integrating spheres under ambient air. To expel the dissolved oxygen, nitrogen gas was perfused through the solution. The delay fluorescence spectra were recorded as a neat film using EPL picosecond pulsed diode lasers as the excitation sources at room temperature. Phosphorescence spectra were measured under nitrogen atmosphere in cryoprobe with microsecond flashlamp as the excitation sources at 77 K. Atomic force microscopy (AFM) images of the thin film were taken by non-contact mode with Park Systems model NX-10. Cyclic voltammetry (CV) was performed on Autolab PGSTAT101 using dichloromethane as solvent under argon atmosphere and tetrabutylammonium hexafluorophosphate (n-Bu$_4$NPF$_6$) as a supporting electrolyte. The HOMO energy level of the neat film was measured by photoelectron spectroscopy (PES) on RIKEN model AC-2 under ambient air. The theoretical calculations were carried out with Gaussian 09 program package.[23] The ground state molecular geometries, HOMO and LUMO distributions, and HOMO, LUMO energy levels of the polymer fragment were computed by the B3LYP/6-31g(d) method. For the excited state calculations, the lowest-lying singlet (S$_1$) and triplet (T$_1$) energy levels were optimized by the TDA-M062X/6-31G(d) method.

The solution-processed OLED devices were fabricated with both non-doped and doped configurations of ITO/PEDOT:PSS (35 nm)/polymer (60 nm)/TmPyPB (40 nm)/LiF (0.5 nm)/Al (100 nm) and ITO/PEDOT:PSS (35 nm)/polymer 5 wt% doped mCP (60 nm)/TmPyPB (40 nm)/LiF (0.5 nm)/Al (100 nm), respectively. The thoroughly cleaned ITO-coated glass substrates were cured with UV ozone for 20 min. The

PEDOT:PSS was spin-coated on the substrates in ambient air, followed by annealing at 160 °C for 30 min. In a nitrogen glove box, the synthesized polymers as a non-doped emissive layer and polymers 5 wt% doped in mCP as a doped emissive layer were dissolved in chlorobenzene. The polymer solutions (2% w/v) were spin-coated on top of the PEDOT:PSS coated ITO substrates at a spin speed of 3000 rpm for 30 seconds to obtain a 60 nm-thick film. Film thickness was measured by Dektak XTL stylus profiler. Then TmPyPB, LiF, and Al were successively coated on top by evaporation technique using Kurt J. Lasker mini SPECTROS 100. The devices were encapsulated with epoxy resin and curing with a UV curing lamp. The EL spectra were recorded by an Ocean Optic USB4000 multi-channel spectrometer in ambient air at room temperature. The current density–voltage–luminance (J–V–L) characteristics were measured by Keithley 2400 source meter and a Hamamatsu Photonics PMA-12 multi-channel analyzer. The absolute external quantum efficiency (EQE) was measured by Hamamatsu Photonics External Quantum Efficiency Measurement C9920-12, utilizing an integrating sphere. All measurements were performed under an ambient atmosphere at room temperature.

Synthesis and characterization

2-(4-(Bis(4-bromophenyl)amino)phenyl)-9H-thioxanthen-9-one-10,10-dioxide (**5**) was synthesized according to literature method.[12g]

2,7-Dibromo-9,9-bis(8-bromooctyl)fluorene (2). The mixture of **1** (3.00 g, 9.26 mmol) and tetrabutylammonium bromide (0.30 g, 0.92 mmol) and KOH (5.19 g, 92.6 mmol) in THF (30 mL) and water (5 mL) were stirred at room temperature for 30 min. Then, 1,8-dibromooctane (8.53 mL, 46.3 mmol) was added, and the mixture was stirred at 70 °C for a further 4 h. The mixture was cool to room temperature and poured into water (100 mL). The mixture was extracted with dichloromethane (3 × 30 mL). The combined organic layer was washed with water, brine solution, dried over with anhydrous Na$_2$SO$_4$, filtered, and evaporated to dryness. The crude product was purified by column chromatography eluting with hexane to give light yellow solids (4.84 g, 74%). ^{1}H NMR (600 MHz, CDCl$_3$) δ 7.52 (d, 2H, $J =$ 7.92 Hz), 7.46 (d, 2H, $J =$ 8.04 Hz), 7.43 (s, 2H), 3.34 (t, 4H, $J =$ 6.72 Hz), 1.91 (t, 4H, $J =$ 7.74 Hz), 1.79–1.75 (m, 4H), 1.33–1.28 (m, 4H), 1.12–1.06 (m, 12H), 0.58 (bs, 4H) ppm. HRMS APCI (m/z) calcd for C$_{29}$H$_{38}$Br$_4$: 705.9666; found 706.9927 (MH$^+$).

9,9′-((2,7-Dibromofluorene)-bis(octane-8,1-diyl))-bis(3,6-di-*tert*-butylcarbazole) (3). A mixture of 3,6-di-*tert*-butylcarbazole (2.22 g, 7.95 mmol) and KOH (1.19 g, 21.20 mmol) in N,N-dimethylformamide (DMF) (28 mL) were stirred at 0 °C. Then **2** (1.87 g, 2.65 mmol) was added in one portion. The mixture was stirred a room temperature overnight and poured into water (100 mL). The mixture was extracted with ethyl acetate (2 × 50 mL). The combined organic phases were washed with water, brine solution, dried over anhydrous Na$_2$SO$_4$, filtered, and evaporated to dryness by column chromatography eluting with hexane followed by recrystallization from hexane/MeOH to afford white solids (2.77 g, 88%). ^{1}H NMR (600 MHz, CDCl$_3$) δ 8.08 ppm (s, 4H), 7.48–7.39 (m, 10H), 7.24 (d, 4H, $J =$ 8.6 Hz),

4.16 (t, 4H), 1.88–1.85 (m, 4H), 1.77–1.72 (m, 4H), 1.45 (s, 36H), 1.28–1.23 (m, 4H), 1.13–1.11 (m, 4H), 1.06–0.97 (m, 8H), 0.54 (s, 4H) ppm; ^{13}C NMR (150 MHz, CDCl$_3$) δ 152.44, 141.39, 139.08, 138.98, 130.21, 126.15, 123.17, 122.67, 121.48, 121.15, 116.23, 108.01, 55.66, 43.13, 40.05, 34.65, 32.09, 29.69, 29.23, 29.07, 28.98, 27.22, 23.53 ppm. HRMS Q-TOF (*m/z*) calcd for C$_{69}$H$_{86}$Br$_2$N$_2$ (M$^+$): 1102.5137; found 1103.5635 (MH$^+$).

Polymerization. A mixture of the monomers 2-(4-(bis(4-bro-mophenyl)amino)phenyl)-9*H*-thioxanthen-9-one-10,10-dioxide (**5**) and 9,9′-((2,7-dibromofluorene)-bis(octane-8,1-diyl))-bis(3,6-di-*tert*-butyl-carbazole) (**3**) in the different molar ratios of 1 : 0, 0.75 : 0.25, 0.50 : 0.50 and 0.25 : 0.75, to of 9-(9-heptadecanyl)-2,7-bis(4,4,5,5-tetramethyl-1,3,2-dioxaborolan-2-yl)carbazole (**6**) (145 mg, 0.221 mmol), trioctylmethyl ammonium chloride (Aliquat 336) (4.45 mg, 0.011 mmol), 2 M Cs$_2$CO$_3$ (aq.) (0.90 mL) and toluene (4 mL) in Schlenk tube was degassed with N$_2$ for 10 min. Then, Pd(PPh$_3$) (8.1 mg, 0.007 mmol) was added, and the mixture was degassed with N$_2$ for another 5 min. The reaction mixture was stirred vigorously under nitrogen at 90 °C for 72 h. It was then poured into methanol (50 mL) and stirred. The precipitate was collected by filtration and washed with 2 M HCl and MeOH, respectively. It was subsequently purified by Soxhlet extraction with acetone followed by chloroform. The chloroform extract was treated with a metal scavenger (Silia-MetS Thiourea) to remove the remaining palladium catalyst and stirred for 2 h at room temperature. The mixture was filtered through a plug of silica eluting with chloroform, and the solvent was removed by a rotary evaporator. The crude product was reprecipitated in methanol, filtrated, and air-dried.

PCTXO (187 mg, 95%) as red solids. M_n = 11 713 Da, PDI = 2.21; ^{1}H NMR (600 MHz, CDCl$_3$) δ 8.57 (d, Ar H), 8.38 (d, Ar H), 8.27–8.11 (m, Ar H), 8.07 (d, Ar H), 7.89 (t, Ar H), 7.83–7.75 (m, Ar H), 7.70 (s, Ar H), 7.67–7.56 (m, Ar H), 7.50 (s, Ar H), 7.43 (d, Ar H), 7.35 (s, Ar H), 7.10 (d, Ar H), 4.69 (s, CH), 2.39 (s, CH$_2$), 2.00 (s, CH$_2$), 1.63 (s, CH$_2$), 1.32–0.99 (m, CH$_2$), 0.79 (t, CH$_3$) ppm.

PCTXO-F25 (283 mg, 70%) as red solids. M_n = 15 628 Da, PDI = 2.39; ^{1}H NMR (600 MHz, CDCl$_3$) δ 8.57 (s, Ar H), 8.38 (d, Ar H), 8.25–8.16 (m, Ar H), 8.08 (d, Ar H), 8.06 (s, Ar H), 7.90 (t, Ar H), 7.84–7.79 (m, Ar H), 7.71 (s, Ar H), 7.64 (d, Ar H), 7.55 (s, Ar H), 7.50 (s, Ar H), 7.41 (d, Ar H), 7.36 (s, Ar H), 7.18 (d, Ar H), 4.69 (s, C$_H$), 4.11 (t, CH$_2$), 2.40 (s, CH$_2$), 2.11 (s, CH$_2$), 1.99 (s, CH$_2$), 1.74 (s, CH$_2$), 1.60 (s, CH$_2$), 1.40 (s, CH$_3$), 1.27–1.14 (m, CH$_2$), 1.22–1.14 (m, CH$_2$), 0.89–0.87 (m, CH$_2$), 0.80 (t, CH$_3$) ppm.

PCTXO-F50 (290 mg, 72%) as red solids. M_n = 17 324 Da, PDI = 2.37; ^{1}H NMR (600 MHz, CDCl$_3$) δ 8.58 (s, Ar H), 8.38 (d, Ar H), 8.25–8.18 (m, Ar H), 8.06 (s, Ar H), 7.89 (t, Ar H), 7.85–7.80 (m, Ar H), 7.71 (s, Ar H), 7.64 (s, Ar H), 7.56 (s, Ar H), 7.50 (s, Ar H), 7.41 (d, Ar H), 7.36 (s, Ar H), 7.18 (d, Ar H), 4.70 (s, CH), 4.11 (s, CH$_2$), 2.40 (s, CH$_2$), 2.12 (s, CH$_2$), 1.97 (s, CH$_2$), 1.72 (s, CH$_2$), 1.57 (s, CH$_2$), 1.42 (s, CH$_3$), 1.26 (s, CH$_2$), 1.14 (s, CH$_2$), 0.86 (br, CH$_2$), 0.80 (s, CH$_3$) ppm.

PCTXO-F75 (315 mg, 78%) as orange solids. M_n = 21 648 Da, PDI = 2.34; ^{1}H NMR (600 MHz, CDCl$_3$) δ 8.58 (s, Ar H), 8.39 (d, Ar H), 8.25–8.18 (m, Ar H), 8.06 (s, Ar H), 7.90–7.80 (m, Ar H), 7.72 (s, Ar H), 7.66–7.65 (m, Ar H), 7.57 (s, Ar H), 7.50 (s, Ar H), 7.42 (d, Ar H), 7.37 (s, Ar H), 7.19 (d, Ar H), 4.70 (s, CH), 4.11 (s, CH$_2$), 2.40 (s, CH$_2$), 2.12 (s, CH$_2$), 1.98 (s, CH$_2$), 1.73 (s, CH$_2$),

1.57 (s, CH$_2$), 1.42 (s, CH$_2$), 1.26–1.24 (m, CH$_2$), 1.18–1.13 (m, CH$_2$), 0.87 (bs, CH$_2$), 0.79 (s, CH$_3$) ppm.

Conflicts of interest

There are no conflicts to declare.

Acknowledgements

Notes and references

1 (a) M. Y. Wong and E. Zysman-Colman, *Adv. Mater.*, 2017, **29**, 1605444; (b) Q. Zhang, J. Li, K. Shizu, S. Huang, S. Hirata, H. Miyazaki and C. Adachi, *J. Am. Chem. Soc.*, 2012, **134**, 14706–14709; (c) K. Shizu, M. Uejima, H. Nomura, T. Sato, K. Tanaka, H. Kaji and C. Adachi, *Phys. Rev. Appl.*, 2015, **3**, 014001; (d) Y. Tao, K. Yuan, T. Chen, P. Xu, H. Li, R. Chen, C. Zheng, L. Zhang and W. Huang, *Adv. Mater.*, 2014, **26**, 7931–7958; (e) M. Godumala, S. Choi, M. J. Cho and D. H. Choi, *J. Mater. Chem. C*, 2019, **7**, 2172–2198; (f) J. Luo, G. Xie, S. Gong, T. Chen and C. Yang, *Chem. Commun.*, 2016, **52**, 2292–2295.

2 (a) X. Yin, Y. He, X. Wang, Z. Wu, E. Pang, J. Xu and J. Wang, *Front. Chem.*, 2020, **8**, 725; (b) J. Kumsampao, C. Chaiwai, P. Chasing, T. Chawanpunyawat, S. Namuangruk, T. Sudyoadsuk and V. Promarak, *Chem.–Asian J.*, 2020, **15**, 3029–3036; (c) M. Godumala, S. Choi, M. J. Cho and D. H. Choi, *J. Mater. Chem. C*, 2016, **4**, 11355–11381.

3 (a) E. Spuling, N. Sharma, I. D. W. Samuel, E. Zysman-Colman and S. Bräse, *Chem. Commun.*, 2018, **54**, 9278–9281; (b) F. Ma, H. Ji, D. Zhang, K. Xue, P. Zhang, Z. Qi and H. Zhu, *Dyes Pigm.*, 2021, **188**, 109208; (c) Z. M. Hudson, J. Poisson, C. M. Tonge, N. R. Paisley, E. R. Sauvé, H. McMillan and S. V. Halldorson, *Macromolecules*, 2021, **54**, 2466–2476; (d) H. Tsujimoto, D. G. Ha, G. Markopoulos, H. S. Chae, M. A. Baldo and T. M. Swager, *J. Am. Chem. Soc.*, 2017, **139**, 4894–4900.

4 (a) K. Wu, T. Zhang, Z. Wang, L. Wang, L. Zhan, S. Gong, C. Zhong, Z. H. Lu, S. Zhang and C. Yang, *J. Am. Chem. Soc.*, 2018, **140**, 8877–8886; (b) M. Mamada, K. Inada, T. Komino, W. J. Potscavage, H. Nakanotani and C. Adachi, *ACS Cent. Sci.*, 2017, **3**, 769–777.

5 (a) J. M. López-De-Luzuriaga, M. Monge, M. E. Olmos, M. Rodríguez-Castillo, I. Soldevilla, D. Sundholm and R. R. Valiev, *Inorg. Chem.*, 2020, **59**, 14236–14244; (b) D. Zhou, W. P. To, G. S. M. Tong, G. Cheng, L. Du, D. L. Phillips and C. M. Che, *Angew. Chem., Int. Ed.*, 2020,

59, 6375–6382; (*c*) J. C. Lima and L. Rodríguez, *Inorganics*, 2019, **7**, 124.

6 (*a*) D. Dou, P. Wu, Z. Liao, J. Hao, J. Zhang and Z. Wang, *RSC Adv.*, 2019, **9**, 23810–23817; (*b*) Z. Wang, H. Wang, J. Zhu, P. Wu, B. Shen, D. Dou and B. Wei, *ACS Appl. Mater. Interfaces*, 2017, **9**, 21346–21354.

7 (*a*) S. J. Woo, Y. Kim, S. K. Kwon, Y. H. Kim and J. J. Kim, *ACS Appl. Mater. Interfaces*, 2019, **11**, 7199–7207; (*b*) H. Tanaka, K. Shizu, H. Miyazaki and C. Adachi, *Chem. Commun.*, 2012, **48**, 11392–11394; (*c*) H. Wang, C. Zang, G. Shan, Z. Yu, S. Liu, L. Zhang, W. Xie and H. Zhao, *Adv. Opt. Mater.*, 2019, **7**, 1801718; (*d*) S. Kothavale, W. J. Chung and J. Y. Lee, *ACS Appl. Mater. Interfaces*, 2020, **12**, 18730–18738; (*e*) C. Li, R. Duan, B. Liang, G. Han, S. Wang, K. Ye, Y. Liu, Y. Yi and Y. Wang, *Angew. Chem., Int. Ed.*, 2017, **56**, 11525–11529; (*f*) T. Huang, D. Liu, J. Jiang and W. Jiang, *Chem.–Eur. J.*, 2019, **25**, 10926–10937.

8 (*a*) J. Rao, C. Zhao, Y. Wang, K. Bai, S. Wang, J. Ding and L. Wang, *ACS Omega*, 2019, **4**, 1861–1867; (*b*) H. Lim, H. J. Cheon, S. J. Woo, S. K. Kwon, Y. H. Kim and J. J. Kim, *Adv. Mater.*, 2020, **32**, 2004083; (*c*) P. Rajamalli, D. Chen, W. Li, I. D. W. Samuel, D. B. Cordes, A. M. Z. Slawin and E. Zysman-Colman, *J. Mater. Chem. C*, 2019, **7**, 6664–6671.

9 (*a*) Y. Xiang, P. Li, S. Gong, Y. H. Huang, C. Y. Wang, C. Zhong, W. Zeng, Z. Chen, W. K. Lee, X. Yin, C. C. Wu and C. Yang, *Sci. Adv.*, 2020, **6**, eaba7855; (*b*) T. A. Lin, T. Chatterjee, W. L. Tsai, W. K. Lee, M. J. Wu, M. Jiao, K. C. Pan, C. L. Yi, C. L. Chung, K. T. Wong and C. C. Wu, *Adv. Mater.*, 2016, **28**, 6976–6983; (*c*) D. R. Lee, B. S. Kim, C. W. Lee, Y. Im, K. S. Yook, S. H. Hwang and J. Y. Lee, *ACS Appl. Mater. Interfaces*, 2015, **7**, 9625–9629; (*d*) D. H. Ahn, S. W. Kim, H. Lee, I. J. Ko, D. Karthik, J. Y. Lee and J. H. Kwon, *Nat. Photonics*, 2019, **13**, 540–546.

10 (*a*) W. Zeng, H. Y. Lai, W. K. Lee, M. Jiao, Y. J. Shiu, C. Zhong, S. Gong, T. Zhou, G. Xie, M. Sarma, K. T. Wong, C. C. Wu and C. Yang, *Adv. Mater.*, 2018, **30**, 1704961; (*b*) J. Liang, C. Li, Y. Cui, Z. Li, J. Wang and Y. Wang, *J. Mater. Chem. C*, 2020, **8**, 1614–1622.

11 J. H. Burroughes, D. D. C. Bradley, A. R. Brown, R. N. Marks, K. Mackay, R. H. Friend, P. L. Burns and A. B. Holmes, *Nature*, 1990, **347**, 539–541.

12 (*a*) Y. Wang, Y. Zhu, G. Xie, H. Zhan, C. Yang and Y. Cheng, *J. Mater. Chem. C*, 2017, **5**, 10715–10720; (*b*) Y. Liu, G. Xie, Z. Ren and S. Yan, *ACS Appl. Polym. Mater.*, 2019, **1**, 2204–2212; (*c*) Y. Wang, Y. Zhu, G. Xie, Q. Xue, C. Tao, Y. Le, H. Zhan and Y. Cheng, *Org. Electron.*, 2018, **59**, 406–413; (*d*) Y. Hu, W. Cai, L. Ying, D. Chen, X. Yang, X. F. Jiang, S. Su, F. Huang and Y. Cao, *J. Mater. Chem. C*, 2018, **6**, 2690–2695; (*e*) J. Rao, X. Liu, X. Li, L. Yang, L. Zhao, S. Wang, J. Ding and L. Wang, *Angew. Chem., Int. Ed.*, 2020, **59**, 1320–1326; (*f*) Y. Zhu, Y. Zhang, B. Yao, Y. Wang, Z. Zhang, H. Zhan, B. Zhang, Z. Xie, Y. Wang and Y. Cheng, *Macromolecules*, 2016, **49**, 4373–4377; (*g*) P. Khammultri, W. Kitisriworaphan, P. Chasing, S. Namuangruk, T. Sudyoadsuk and V. Promarak, *Polym. Chem.*, 2021, **12**, 1030–1039; (*h*) Y. Liu, S. Yan and Z. Ren, *Chem. Eng. J.*, 2020, **417**, 128089.

13 (*a*) X. Liu, J. Rao, X. Li, S. Wang, J. Ding and L. Wang, *iScience*, 2019, **15**, 147–155; (*b*) H. J. Kim, C. Lee, M. Godumala, S. Choi, S. Y. Park, M. J. Cho, S. Park and D. H. Choi, *Polym. Chem.*, 2018, **9**, 1318–1326; (*c*) A. E. Nikolaenko, M. Cass, F. Bourcet, D. Mohamad and M. Roberts, *Adv. Mater.*, 2015, **27**, 7236–7240; (*d*) S. Y. Lee, T. Yasuda, H. Komiyama, J. Lee and C. Adachi, *Adv. Mater.*, 2016, **28**, 4019–4024.

14 (*a*) Z. Ren, R. S. Nobuyasu, F. B. Dias, A. P. Monkman, S. Yan and M. R. Bryce, *Macromolecules*, 2016, **49**, 5452–5460; (*b*) C. Li, Y. Xu, Y. Liu, Z. Ren, Y. Ma and S. Yan, *Nano Energy*, 2019, **65**, 104057; (*c*) C. Li, R. S. Nobuyasu, Y. Wang, F. B. Dias, Z. Ren, M. R. Bryce and S. Yan, *Adv. Opt. Mater.*, 2017, **5**, 1700435; (*d*) Y. Yang, L. Zhao, S. Wang, J. Ding and L. Wang, *Macromolecules*, 2018, **51**, 9933–9942; (*e*) X. Zhou, M. Huang, X. Zeng, T. Chen, G. Xie, X. Yin and C. Yang, *Polym. Chem.*, 2019, **10**, 4201–4208.

15 (*a*) S. Shao, J. Hu, X. Wang, L. Wang, X. Jing and F. Wang, *J. Am. Chem. Soc.*, 2017, **139**, 17739–17742; (*b*) J. Hu, Q. Li, X. Wang, S. Shao, L. Wang, X. Jing and F. Wang, *Angew. Chem., Int. Ed.*, 2019, **58**, 8405–8409.

16 (*a*) Y. Li, T. Chen, M. Huang, Y. Gu, S. Gong, G. Xie and C. Yang, *J. Mater. Chem. C*, 2017, **5**, 3480–3487; (*b*) X. Ban, W. Jiang, T. Lu, X. Jing, Q. Tang, S. Huang, K. Sun, B. Huang, B. Lin and Y. Sun, *J. Mater. Chem. C*, 2016, **4**, 8810–8816; (*c*) K. Sun, D. Chu, Y. Cui, W. Tian, Y. Sun and W. Jiang, *Org. Electron.*, 2017, **48**, 389–396; (*d*) K. Sun, Y. Sun, D. Liu, Y. Feng, X. Zhang, Y. Sun and W. Jiang, *Dyes Pigm.*, 2017, **147**, 436–443.

17 (*a*) T. Jiang, Y. Liu, Z. Ren and S. Yan, *Polym. Chem.*, 2020, **11**, 1555–1571; (*b*) Q. Wei, Z. Ge and B. Voit, *Macromol. Rapid Commun.*, 2019, **40**, 1800570.

18 S. R. Forrest, *Nature*, 2004, **428**, 911–918.

19 H. Wang, L. Xie, Q. Peng, L. Meng, Y. Wang, Y. Yi and P. Wang, *Adv. Mater.*, 2014, **26**, 5198–5204.

20 (*a*) J. F. Morin and M. Leclerc, *Macromolecules*, 2002, **35**, 8413–8417; (*b*) R. He, S. Hu, J. Liu, L. Yu, B. Zhang, N. Li, W. Yang, H. Wu and J. Peng, *J. Mater. Chem.*, 2012, **22**, 3440–3446; (*c*) F. Dumur, *Org. Electron.*, 2015, **25**, 345–361.

21 (*a*) W. Kitisriworaphan, T. Chawanpunyawat, T. Manyum, P. Chasing, S. Namuangruk, T. Sudyoadsuk and V. Promarak, *RSC Adv.*, 2021, **11**, 12710–12719; (*b*) Y. Thathong, P. Chasing, T. Manyum, S. Namuangruk, S. Saengsuwan, T. Sudyoasuk and V. Promarak, *New J. Chem.*, 2021, **45**, 7694–7704.

22 L. Hao, M. Wang, W. Shan, C. Deng, W. Ren, Z. Shi and H. Lü, *J. Hazard. Mater.*, 2017, **339**, 216–222.

23 M. J. Frisch, G. W. Trucks, H. B. Schlegel, G. E. Scuseria, M. A. Robb, J. R. Cheeseman, G. Scalmani, V. Barone, G. A. Petersson, H. Nakatsuji, X. Li, M. Caricato, A. V. Marenich, J. Bloino, B. G. Janesko, R. Gomperts, B. Mennucci, H. P. Hratchian, J. V. Ortiz, A. F. Izmaylov, J. L. Sonnenberg, Williams, F. Ding, F. Lipparini, F. Egidi, J. Goings, B. Peng, A. Petrone, T. Henderson, D. Ranasinghe, V. G. Zakrzewski, J. Gao, N. Rega, G. Zheng, W. Liang, M. Hada, M. Ehara, K. Toyota, R. Fukuda, J. Hasegawa, M. Ishida, T. Nakajima, Y. Honda,

O. Kitao, H. Nakai, T. Vreven, K. Throssell, J. A. Montgomery, Jr, J. E. Peralta, F. Ogliaro, M. J. Bearpark, J. J. Heyd, E. N. Brothers, K. N. Kudin, V. N. Staroverov, T. A. Keith, R. Kobayashi, J. Normand, K. Raghavachari, A. P. Rendell, J. C. Burant, S. S. Iyengar, J. Tomasi, M. Cossi, J. M. Millam, M. Klene, C. Adamo, R. Cammi, J. W. Ochterski, R. L. Martin, K. Morokuma, O. Farkas, J. B. Foresman and D. J. Fox, *Gaussian 09, Revision A.02*, Gaussian, Inc., 2016.

24 M. Kumar and L. Pereira, *ACS Omega*, 2020, **5**, 2196–2204.

25 V. Sannasi and D. Jeyakumar, *Des. Monomers Polym.*, 2016, **19**, 719–729.

26 G. Tu, Q. Zhou, Y. Cheng, L. Wang, D. Ma, X. Jing and F. Wang, *Appl. Phys. Lett.*, 2004, **85**, 2172–2174.

27 (*a*) Y. Wang, Y. Zhu, X. Lin, Y. Yang, B. Zhang, H. Zhan, Z. Xie and Y. Cheng, *J. Mater. Chem. C*, 2018, **6**, 568–574; (*b*) J. Huang, Y. Niu, W. Yang, Y. Mo, M. Yuan and Y. Cao, *Macromolecules*, 2002, **35**, 6080–6082.

28 Q. Wei, P. Kleine, Y. Karpov, X. Qiu, H. Komber, K. Sahre, A. Kiriy, R. Lygaitis, S. Lenk, S. Reineke and B. Voit, *Adv. Funct. Mater.*, 2017, **27**, 1605051.

29 (*a*) P. Lundberg, Y. Tsuchiya, E. M. Lindh, S. Tang, C. Adachi and L. Edman, *Nat. Commun.*, 2019, **10**, 5307; (*b*) R. S. Nobuyasu, Z. Ren, G. C. Griffiths, A. S. Batsanov, P. Data, S. Yan, A. P. Monkman, M. R. Bryce and F. B. Dias, *Adv. Opt. Mater.*, 2016, **4**, 597–607.

30 (*a*) P. C. Kao, J. H. Lin, J. Y. Wang, C. H. Yang and S. H. Chen, *J. Appl. Phys.*, 2011, **109**, 094505; (*b*) C. J. Zheng, J. Ye, M. F. Lo, M. K. Fung, X. M. Ou, X. H. Zhang and C. S. Lee, *Chem. Mater.*, 2012, **24**, 643–650; (*c*) N. B. Kotadiya, H. Lu, A. Mondal, Y. Ie, D. Andrienko, P. W. M. Blom and G. J. A. H. Wetzelaer, *Nat. Mater.*, 2018, **17**, 329–334.

31 (*a*) Y. Li, T. Dutta, N. Gerasimchuk, S. Wu, K. Shetye, L. Jin, R. Wang, D. M. Zhu and Z. Peng, *ACS Appl. Mater. Interfaces*, 2015, **7**, 9372–9384; (*b*) M. Nikolka, K. Broch, J. Armitage, D. Hanifi, P. J. Nowack, D. Venkateshvaran, A. Sadhanala, J. Saska, M. Mascal, S. H. Jung, J. K. Lee, I. McCulloch, A. Salleo and H. Sirringhaus, *Nat. Commun.*, 2019, **10**, 2122.

32 (*a*) S. W. Culligan, A. C. A. Chen, J. U. Wallace, K. P. Klubek, C. W. Tang and S. H. Chen, *Adv. Funct. Mater.*, 2006, **16**, 1481–1487; (*b*) R. A. K. Yadav, D. K. Dubey, S. Z. Chen, T. W. Liang and J. H. Jou, *Sci. Rep.*, 2020, **10**, 9915; (*c*) P. Therdkatanyuphong, P. Chasing, C. Kaiyasuan, S. Boonnab, T. Sudyoadsuk and V. Promarak, *Adv. Funct. Mater.*, 2020, **30**, 2002481.

33 (*a*) A. Kumar, W. Lee, T. Lee, J. Jung, S. Yoo and M. H. Lee, *J. Mater. Chem. C*, 2020, **8**, 4253–4263; (*b*) F. M. Xie, P. Wu, S. J. Zou, Y. Q. Li, T. Cheng, M. Xie, J. X. Tang and X. Zhao, *Adv. Electron. Mater.*, 2020, **6**, 1900843; (*c*) B. Li, Z. Li, T. Hu, Y. Zhang, Y. Wang, Y. Yi, F. Guo and L. Zhao, *J. Mater. Chem. C*, 2018, **6**, 2351–2359.

© 2021 The Author(s). Published by the Royal Society of Chemistry